



Dynamics of structural and magnetic phase transitions in ferroborate $\text{YFe}_3(\text{BO}_3)_4$

K.V. Frolov ^{a,*}, I.S. Lyubutin ^a, O.A. Alekseeva ^a, E.S. Smirnova ^a, I.A. Verin ^a, V.L. Temerov ^b, L.N. Bezmaternykh ^b, I.A. Gudim ^b, V.V. Artemov ^a, T.V. Dmitrieva ^a

^a Shubnikov Institute of Crystallography of FRC “Crystallography and Photonics” RAS, 119333 Moscow, Russia

^b Kirensky Institute of Physics, Siberian Branch of Russian Academy of Sciences, 660036 Krasnoyarsk, Russia



ARTICLE INFO

Article history:

Received 2 November 2017

Received in revised form

17 March 2018

Accepted 19 March 2018

Available online 20 March 2018

Keywords:

Multiferroics

Rare-earth compounds

X-ray diffraction

Mössbauer spectroscopy

Crystal structure

ABSTRACT

X-ray analysis of the $\text{YFe}_3(\text{BO}_3)_4$ single crystal revealed different behavior of parameters of the crystal cell with an increase in temperature from 25 to 500 K. The parameters a and b initially increase monotonically and then rise sharply in the range between 360 and 380 K, which corresponds to the structural phase transition. The parameter c initially decreases linearly upon heating and then begins to increase, passing through a minimum at 90 K. In the interval of 200–500 K the parameter c grows linearly and does not undergo anomalies at the structural phase transition. The results of Mössbauer measurements at ^{57}Fe nuclei in the paramagnetic phase of $\text{YFe}_3(\text{BO}_3)_4$ correlate well with the XRD data, but they do not separate the two structural states of iron ions Fe1 and Fe2 arising in the $P3_{1}21$ phase during the structural phase transition. The temperature of the magnetic phase transition $T_N = 39.42(16)$ K is established, below which the iron ions form a 3D magnetic order of the Heisenberg type. The calculated “Mössbauer” Debye temperature $\Theta_M = 340(2)$ K turned out to be three times lower than the Debye temperature of the entire crystal lattice $T_D = 1020$ K. Mössbauer data indicate a weak bonding between the helicoidal chains of iron and the rest of the crystal lattice.

© 2018 Elsevier B.V. All rights reserved.

1. Introduction

Ferroelectromagnetic [1] or multiferroic [2] materials have attracted a lot of attention in the last 10 years due to their coexistence and interrelation of ferroelectric and magnetic ordering [3–5]. The practical importance of multiferroic materials for magnetic recording, sensors, spintronic and energy conversion devices is well-known [5–7], however, only a few compounds have sufficiently high critical parameters appropriate for practical use. The undoped and doped bismuth-ferrite BiFeO_3 [8–12] and rare-earth manganites RMnO_3 ($R = \text{Y}, \text{La}, \text{Pr-Er}$) [13–16] are the most famous. The high excitement was caused by the discovery of a novel class of multiferroics in which ferroelectricity exists only in a magnetically ordered state [17–23]. In particular, some of the rare-earth ferroborates $R\text{Fe}_3(\text{BO}_3)_4$ belong to these compounds. While they do not have the high critical parameters essential for practical applications, but they are interesting as model objects with two

magnetic subsystems of iron and rare-earth ions. Ferroborates demonstrate the variety of properties and phase transitions depending on the type of rare-earth elements in their composition [24–31]. From this point of view, the $\text{YFe}_3(\text{BO}_3)_4$ compound containing only one magnetic subsystem of iron ions is of special interest. It exhibits a low-temperature magnetic phase transition at $T_N \approx 40$ K and a high-temperature structural phase transition, but the literature data on the temperature of structural transition (T_S) differ strongly. Measurements of the heat capacity of polycrystalline $\text{YFe}_3(\text{BO}_3)_4$ sample [32] indicate the transition at $T_S = 445$ K, but later experiments on single-crystal samples show $T_S = 350$ K [33] and 401 K [34], respectively.

In the present work, the dynamics of phase transitions in a single crystal of $\text{YFe}_3(\text{BO}_3)_4$ in the temperature range 5–500 K was studied by X-ray diffraction (XRD) and Mössbauer spectroscopy methods and the transition temperatures T_N and T_S were established.

2. Experimental details

High-quality single crystals of $\text{YFe}_3(\text{BO}_3)_4$ were grown from the

* Corresponding author.

E-mail addresses: green@crys.ras.ru, k.v.frolov@gmail.com (K.V. Frolov).

bismuth trimolibdate-melt solution by the procedure described in detail in Refs. [35,36]. The elemental chemical composition of the single crystal was determined by an energy-dispersive X-ray microanalysis using an FEI Quanta 200 3D Dual Beam scanning electron microscope equipped with an EDAX microanalyzer at an accelerating voltage of 30 kV. Bismuth atoms Bi were found in the sample in an amount of about 2% by weight, which can enter the crystal from the solution (melt) during the synthesis process, presumably substituting yttrium Y atoms in the structure.

The XRD studies of the lattice parameters of $\text{YFe}_3(\text{BO}_3)_4$ single crystals were performed in the temperature range 30–500 K by several methods. The measurements in the range of 30–220 K in steps of 5–10° and at room temperature of 295 K were performed on the four-circle HUBER-5042 diffractometer equipped with a closed-cycle helium cryostat DISPLEX DE-202 according to the procedure described in Refs. [37,38]. The measurements in the interval 110–500 K were taken in steps of 10–20° at the SNBL station of the European Synchrotron Radiation Facility (ESRF, beamline ID-01) with a PILATUS@SNBL diffractometer [39] using an Oxford Cryostream 700 + temperature attachment in a laminar nitrogen gas stream. Additional measurements between 295 and 500 K were performed on a four-circle X-ray Rigaku Oxford Diffraction CCD Xcalibur S diffractometer equipped with an Oxford Cryosystems Cobra Plus temperature device also in a laminar flow of nitrogen gas.

To conduct Mössbauer experiments, we prepared the powder samples with a mass of 30(1) mg from single crystals. For this purpose, small parts of single crystals were pre-ground in an agate mortar, then, the resulting powder was poured into a thin-walled cylindrical container 8 mm in diameter from thin aluminum foil and pressed lightly. Mössbauer absorption spectra at ^{57}Fe nuclei were obtained in the temperature range 5–480 K on standard MS-1104Em spectrometer equipped with the closed-cycle helium cryostat RTI CryoFree-104 [40] and the high-temperature resistive MRF-750K furnace. The gamma-ray source ^{57}Co (Rh) was at room temperature. The values of isomer shifts were measured relative to a standard absorber (metallic α -Fe at room temperature). The computer analysis of spectra was performed using the program Univem MS - the supplied software of the MS-1104Em spectrometer, and the SpectrRelax program [41].

3. Results and discussion

3.1. X-ray research data

The crystals of rare-earth ferroborates are isostructural to the natural mineral huntite $\text{CaMg}_3(\text{CO}_3)_4$ and have the trigonal symmetry with the sp.gr. $R\bar{3}2(D^7_{3h})$ [42,43]. The crystal structure of the high-temperature phase of $\text{YFe}_3(\text{BO}_3)_4$ with the symmetry group $R\bar{3}2$ observed at temperatures $T > 445$ K is given in Fig. 1. Atomic layers consisting of trigonal prisms YO_6 and smaller FeO_6 octahedra are located perpendicular to the c axis (C_3). The boron atoms form with the oxygen atoms triangles $[\text{BO}_3]^{3-}$ of two types. Triangles of the first type $[\text{BO}_3]1$ are connected by vertices only with FeO_6 octahedra, and the other triangles $[\text{BO}_3]2$ are connected by one vertex to two FeO_6 octahedra, and each of other two vertices is connected to the FeO_6 octahedron and the prism YO_6 . Octahedra FeO_6 are joined by edges and form helical chains elongated along the c axis [43]. In the high-temperature phase (at $T > 445$ K), only one structural position of iron ions exists, and all FeO_6 chains are equivalent. When cooling during the structural phase transition, a decrease in the crystal symmetry occurs from the sp.gr. $R\bar{3}2$ to sp.gr. $P\bar{3}121$, and two non-equivalent positions of iron ions $\text{Fe}1$ and $\text{Fe}2$ should appear [33,44]. These ions form two types of helical FeO_6 chains, similar to that observed in gadolinium ferroborate $\text{GdFe}_3(\text{BO}_3)_4$ [45,46].

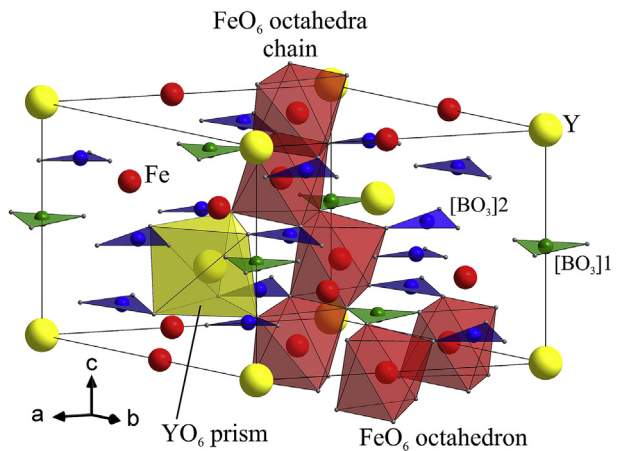


Fig. 1. Crystal structure of ferroborate $\text{YFe}_3(\text{BO}_3)_4$ in the high-temperature phase with a sp.gr. $R\bar{3}2$. Iron atoms occupy one type of sites. Green oxygen triangles containing boron atoms $[\text{BO}_3]$ are connected by vertices only with octahedra FeO_6 (type $[\text{BO}_3]1$). In the blue triangles $[\text{BO}_3]2$, one vertex is connected to two octahedra FeO_6 , and each of the other two vertices are connected to the octahedron FeO_6 and the prism YO_6 . (For interpretation of the references to colour in this figure legend, the reader is referred to the Web version of this article.)

Fig. 2 shows the temperature behavior of crystal lattice parameters obtained from XRD data for the $\text{YFe}_3(\text{BO}_3)_4$ crystal in the temperature range 30–500 K. It is seen that a and b cell parameters

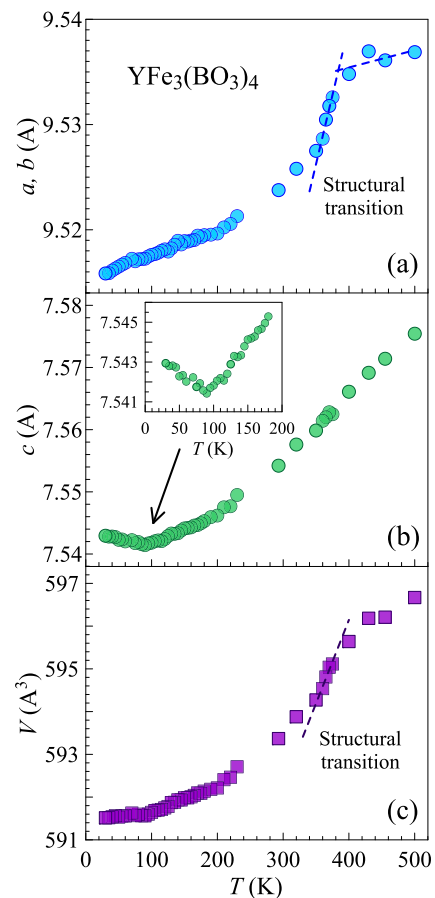


Fig. 2. Temperature variation of the unit cell parameters a , b and c (a,b), and the unit cell volume (c) in $\text{YFe}_3(\text{BO}_3)_4$ crystal. The area of anomalous behavior of the c parameter is shown in the inset of figure (b) on an enlarged scale. The errors are within the points. Dashed lines are guides for the eye indicating the structural transition.

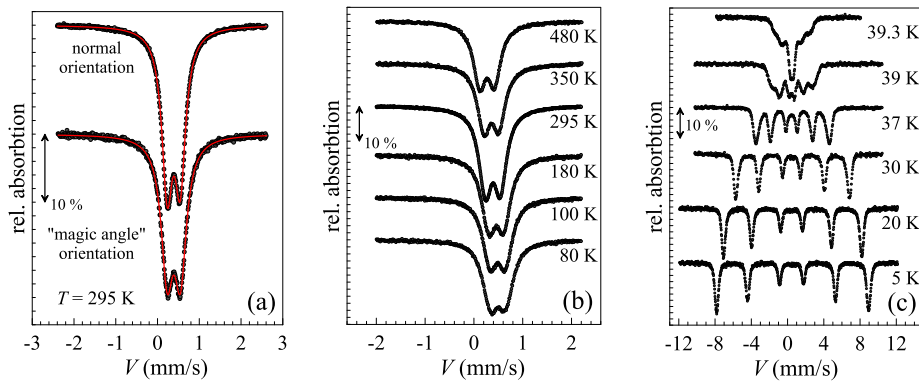


Fig. 3. Mössbauer spectra of $\text{YFe}_3(\text{BO}_3)_4$ compound at different temperatures: (a) at $T = 295$ K, the upper spectrum - the plane of absorber is perpendicular to the propagation vector of γ -rays k_γ , the lower spectrum - the plane of absorber is rotated to the "magic angle" $\alpha = 54.7^\circ$ to the direction of k_γ ; (b) at temperatures above the point of magnetic phase transition $T_N = 39.5$ K; (c) at $T < T_N = 39.5$ K.

increase monotonically with increasing temperature in the range 30–360 K (Fig. 2a). A sharp increase of a and b values occurs in the range 360–380 K. However, the rise of these parameters practically ceases with further heating in the region of 400–500 K. We assume that the main structural transformation occurs in the range between 360 and 380 K.

The cell parameter c behaves differently (Fig. 2b). When heating from 30 K, it decreases anomalously by ≈ 0.002 Å and reaches a minimum value at 90 K. The parameter c practically grows linearly with a further increase of the temperature to 500 K, and the temperature dependence $c(T)$ shows no apparent anomalies even in the region of structural phase transition. This behavior of the c parameter may be due to the weak coupling of the helicoidal chains of FeO_6 with the main crystal lattice. It should be noted that we detected an analogous behavior of the c parameter in the 90 K region in the single crystal $\text{GdFe}_3(\text{BO}_3)_4$ [37], where a structural phase transition is observed at about 155 K. The unit cell volume in YFe_3BO_3 rises smoothly with an increase in temperature, and shows a steeper rise in the region of the structural transition at 360–380 K (Fig. 2c).

It was revealed earlier [47] that low-temperature (at $T < 150$ K) anomalies of elastic constants, for example, softening of Young's modulus, can be observed in rare-earth ferroborates. These anomalies are associated with the energy spectrum and wave functions of rare-earth ions, with the symmetry of their local environment and f - d interaction with the subsystem of Fe^{3+} ions. But in our case the $\text{YFe}_3(\text{BO}_3)_4$ compound does not contain rare-earth ions, and the observed anomalous behavior of cell parameters may indicate a special role of exchange interactions within the iron sub-system. This conclusion is in a good agreement with well-known fact that the magnetic superexchange $\text{Fe}-\text{O}-\text{Fe}$ (through one oxygen) in chains along the c -axis of ferroborates is much stronger than superexchanges in ab -planes between iron ions and/or between iron and rare-earth ions, occurring via the paths $\text{Fe}-\text{O}-\text{O}-\text{Fe}$, $\text{Fe}-\text{O}-\text{R}$, $\text{Fe}-\text{O}-\text{O}-\text{R}$ and $\text{R}-\text{O}-\text{O}-\text{R}$ [33,34]. This is also confirmed by the proximity of the values of the Neel temperature in ferroborates with various rare earth elements [24].

To determine the causes of observed anomalies, we carried out detailed low-temperature structural studies of $\text{YFe}_3(\text{BO}_3)_4$ single crystals, and the results will be presented in the next article.

3.2. Mossbauer spectroscopy data

3.2.1. High-temperature region

The Mössbauer spectrum of $\text{YFe}_3(\text{BO}_3)_4$ crystal at room temperature is a slightly asymmetric paramagnetic doublet (the upper

spectrum in Fig. 3a), which is analogous in shape and parameters to the spectrum observed in the $\text{GdFe}_3(\text{BO}_3)_4$ crystal [37]. We recall that at room temperature the crystal lattice of $\text{GdFe}_3(\text{BO}_3)_4$ has already undergone a structural phase transition at $T_S \approx 155$ K. At 295 K, it is described by the space group $R\bar{3}2$ (D_{3h}^7), where Fe^{3+} ions are in only one site. Meanwhile, the lattice of $\text{YFe}_3(\text{BO}_3)_4$ crystal at 295 K should be described by the space group $P\bar{3}121$, and contains two non-equivalent sites of iron ions, $\text{Fe}1$ and $\text{Fe}2$, forming two types of helical chains FeO_6 .

Therefore, in order to elucidate the reason for the doublet asymmetry in the $\text{YFe}_3(\text{BO}_3)_4$ spectrum (and the possible relation of this effect to the presence of two iron sites), we performed additional measurements of Mössbauer spectrum when the sample plane was oriented under a "magic angle" ($\alpha = 54.7^\circ$) to the direction of propagation of the γ -radiation. Such geometry allows to exclude the texture effect (to the shape of a spectrum), which may arise when preparing a powder sample from crushed single crystals, if powder particles are obtained in the form of plates and/or rods [48].

As is seen in the lower spectrum of Fig. 3a, the asymmetry of lines disappears when the sample is oriented under the "magic angle". The spectrum is well described by a single symmetrical doublet with the hyperfine parameters characteristic of the octahedral oxygen coordination of iron ions Fe^{3+} (see Table 1). Thus, a weak asymmetry of the doublet is a texture effect and is not related to two non-equivalent sites of iron ions $\text{Fe}1$ and $\text{Fe}2$. In the all

Table 1
Hyperfine parameters, obtained from Mössbauer spectra of $\text{YFe}_3(\text{BO}_3)_4$ at certain temperatures.

T (K)	δ (mm/s)	Δ (mm/s)	G (mm/s)	$\langle B_{hf} \rangle$ (T)
<i>Doublet</i>				
480	0.270(1)	0.307(1)	0.317(1)	–
420	0.309(1)	0.312(1)	0.320(1)	–
350	0.356(1)	0.310(1)	0.326(1)	–
295	0.388(1)	0.310(1)	0.315(1)	–
*295	0.390(1)	0.320(1)	0.349(1)	–
180	0.455(1)	0.310(1)	0.349(1)	–
100	0.485(1)	0.315(1)	0.354(1)	–
80	0.493(1)	0.317(1)	0.380(2)	–
<i>Magnetic splitting</i>				
30	0.503(2)	0.060(1)	–	37.85(5)
20	0.502(1)	0.060(1)	–	46.98(3)
7.5	0.501(1)	0.058(1)	–	51.57(1)
5	0.503(1)	0.058(1)	–	51.91(2)

δ is the isomer shift, Δ is the quadrupole splitting, G is the line width, * - «magic angle» sample orientation, $\langle \cdot \rangle$ is the average value of quadrupole shift, $\langle B_{hf} \rangle$ is the average value of magnetic hyperfine field at Fe nuclei.

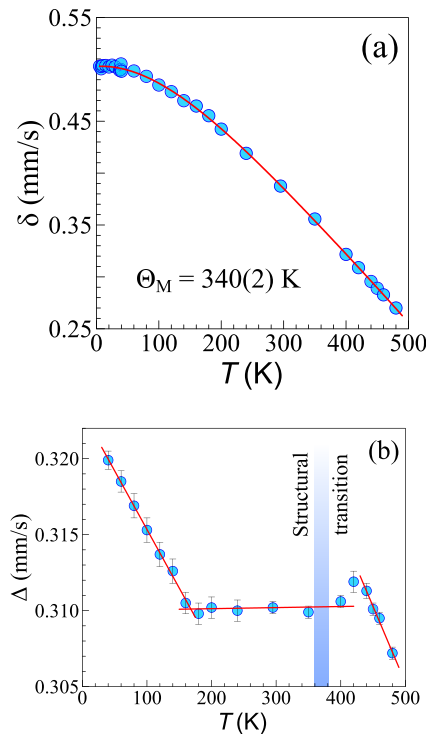


Fig. 4. Temperature dependences of (a) isomer shift $\delta(T)$. The solid red line is the calculated curve obtained in the approximation of the second-order Doppler effect; (b) quadrupole splitting $\Delta(T)$; solid lines are guides for the eye. (For interpretation of the references to colour in this figure legend, the reader is referred to the Web version of this article.)

temperature range of 40–480 K, the Mössbauer spectra of $\text{YFe}_3(\text{BO}_3)_4$ are analogous to the “room” spectrum (Fig. 3b). Thus, the Mössbauer spectra in the paramagnetic region (at $T > 40$ K) do not distinguish between two nonequivalent structural sites of iron ions. The same result was obtained earlier for the $\text{GdFe}_3(\text{BO}_3)_4$ crystal [37].

At the temperature below 180 K spectral lines of the paramagnetic doublet demonstrate certain broadening (Fig. 3b). Note that according to our XRD data (Fig. 2), the dynamics of the unit-cell parameters a and c changes in the range of 180–200 K, namely, the slope in the dependence of $a,b(T)$ and $c(T)$ varies. As seen in Fig. 4b, at the same temperature, a sharp bend occurs of the temperature dependence of the quadrupole splitting parameter $\Delta(T)$ of the Mössbauer doublet, and its linear increase begins with a decrease in temperature.

The anomalous behavior of Mössbauer spectra in $\text{YFe}_3(\text{BO}_3)_4$ was observed in Ref. [49], where the magnetic splitting of the spectra was retained even above the magnetic phase transition point ($T_N \approx 37$ K) to temperatures above 60 K. In addition, instead of the paramagnetic doublet, a single line was observed at 70 K. These results were explained by the spin relaxation effect.

As shown below, such anomalous behavior of low-temperature Mössbauer spectra was not observed in our experiments, and the characteristic magnetic sextet, as expected, was transformed into a paramagnetic doublet at a Neel temperature of $T_N \approx 39.5$ K (see Figs. 3c and 5). In our opinion, to fully understand and theoretically describe the relaxation processes in the spin system of iron ions in $\text{YFe}_3(\text{BO}_3)_4$, it is necessary to conduct additional thorough Mössbauer measurements in the temperature range 30–180 K.

Fig. 4 shows the temperature dependence of the parameters of isomer shift $\delta(T)$ and quadrupole splitting $\Delta(T)$ of the paramagnetic doublet. The behavior of $\delta(T)$ is characteristic of the second order

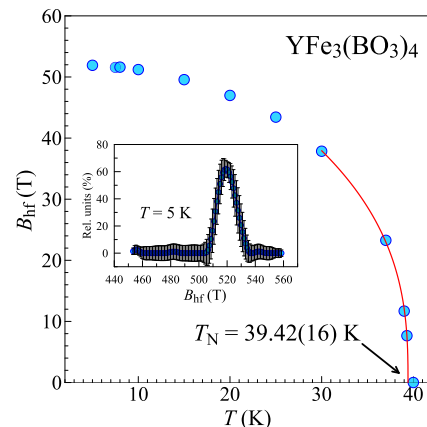


Fig. 5. Temperature dependence of the magnetic hyperfine field B_{hf} at iron nuclei in the $\text{YFe}_3(\text{BO}_3)_4$ crystal. The solid red line is the calculated curve. The inset shows the distribution function of the field B_{hf} at 5 K. (For interpretation of the references to colour in this figure legend, the reader is referred to the Web version of this article.)

Doppler effect. The δ values are 0.498 (1) mm/s at 40 K and 0.387 (1) mm/s at 295 K, which is typical of the high-spin state of Fe^{3+} ions in the octahedral oxygen environment. Using the $\delta(T)$ dependence, we calculated by the standard procedure [50,51] the “Mössbauer” Debye temperature $\Theta_M = 340(2)$ K for the iron sublattice in $\text{YFe}_3(\text{BO}_3)_4$. Interestingly, this value turned out to be three times lower than the characteristic Debye temperature $T_D = 1020$ K, which was previously estimated for the entire $\text{YFe}_3(\text{BO}_3)_4$ crystal [34]. Apparently, this indicates a relatively weak bond between iron ions and the core of crystal lattice.

The temperature dependence of quadrupole parameter $\Delta(T)$ demonstrates a more complex behavior (Fig. 4b). In the paramagnetic region, the Δ value slightly decreases linearly from 0.32 to 0.31 mm/s with a temperature increase from 40 to 160 K. Apparently, when heating, the local distortions of oxygen octahedra containing iron decrease slightly, and the octahedra become more symmetrical, that correlates with the increase of a and b parameters (Fig. 2a).

The value $\Delta \approx 0.31$ mm/s remains practically constant in the temperature range 160–400 K, but the parameter Δ begins to increase above 400 K and reaches a maximum value at $T \approx 420$ K. Then the parameter Δ decreases linearly with further heating up to 480 K (Fig. 4b). We note that, according to our XRD data, a structural phase transition is expected to be in the range 360–380 K (Fig. 2a), which is slightly lower than the temperature anomaly of parameter Δ .

We recall that earlier, when measuring the heat capacity of powder and single-crystal $\text{YFe}_3(\text{BO}_3)_4$ samples, different temperature values were obtained for the structural phase transition T_S in the range 350–445 K [32–34]. In particular, the value $T_S = 401$ K was obtained in Ref. [34], and it was found that the peak on the temperature dependence of heat capacity $C_p(T)$ corresponding to the region of structural transformation is located between $T = 376$ K and 426 K (i.e., $\Delta T = 50$ K). Such a value of ΔT , in the opinion of authors, indicates a second-order phase transition, that agrees with our structural and Mössbauer data. To summarize, we can state that the general change in the symmetry of $\text{YFe}_3(\text{BO}_3)_4$ crystal lattice during the structural phase transition has a very little influence on the local environment of iron ions in oxygen octahedra.

3.2.2. Low-temperature region

Mössbauer spectra below 40 K exhibit a characteristic magnetic splitting (Fig. 3c), which indicates a magnetic ordering of iron ions.

Table 2

The values of parameter β for the different d and n .

d	3	3	3	2
n	1	2	3	1
β	0.31	0.33	0.35	0.125

At low temperatures, the spectra are represented by one magnetic six-lines component without visible splitting into two sublattices. The best approximation of the spectra is achieved by using the Gaussian distribution of Mössbauer hyperfine parameters [52]. The inset in Fig. 5 shows the distribution function $P(B)$ of the magnetic hyperfine field B_{hf} at iron nuclei, calculated by the SpectrRelax program [41]. The distribution is expressed by a single maximum, indicating that all iron atoms have very close values of the magnetic parameters (one sublattice). Thus, in borate $\text{YFe}_3(\text{BO}_3)_4$, even at temperatures below the magnetic phase transition, it is not possible to separate the contributions of the two structural positions of Fe1 and Fe2 ions (Fig. 5).

The previously performed low-temperature ($T = 2$ K) neutron diffraction measurements [53] also made it impossible to separate the magnetic moments of iron ions in the structural sites Fe1 and Fe2 within the error limit. We recall that earlier in the borate $\text{GdFe}_3(\text{BO}_3)_4$, we were able to separate the contributions of Fe1 and Fe2 sites in the Mössbauer spectra at temperatures $T < T_N$, although in the paramagnetic region these contributions were also indistinguishable as in $\text{YFe}_3(\text{BO}_3)_4$ [37]. Apparently, in the absence of a magnetic subsystem of rare-earth ions, the structural and magnetic states of iron ions in sites Fe1 and Fe2 differ a little. This leads to only minor distortions of the local environment in both sites and is manifested only in a small broadening of the Mössbauer spectra.

Fig. 5 shows the temperature dependence of the average value of the magnetic hyperfine field $\langle B_{hf} \rangle$ at ${}^{57}\text{Fe}$ nuclei for iron ions in $\text{YFe}_3(\text{BO}_3)_4$. The experimental dependence of $B_{hf}(T)$ near T_N was approximated by the calculated curve using the model of critical coefficients $B(T) = B_0(1 - T/T_N)^\beta$ [54], in order to clarify the temperature of the magnetic phase transition T_N and determine the type and dimension of the magnetic ordering.

In general, the behavior of magnetic systems can be characterized by the dimension of magnetic lattice d and the dimension of order parameter n . The parameter d can take on values 1 (one-dimensional chains), 2 (layered structure or surface) and 3 (bulk material) (see, for example [55,56]). The parameter n is determined by the model describing the magnetic system, i.e., the form of Hamiltonian H .

$$\begin{aligned} \text{For } n = 1 (\text{Ising model}) : \quad H &= - \sum J_{ij} S^z_i S^z_j; \\ \text{for } n = 2 (\text{planar XY model}) : \quad H &= - \sum J_{ij} (S^x_i S^x_j + S^y_i S^y_j); \\ \text{for } n = 3 (\text{Heisenberg model}) : \quad H &= - \sum J_{ij} \mathbf{S}_i \cdot \mathbf{S}_j. \end{aligned} \quad (1)$$

A long-range order for all n exists only at $d = 3$. The Ising model ($n = 1$) admits a two- and three-dimensional long-range order, while the low-dimensional order ($d = 1$ and 2) is absent in the Heisenberg ($n = 3$) and XY ($n = 2$) models. The values of parameter β in accordance with the model of critical coefficients are given in Table 2.

As a result of the calculations for the $\text{YFe}_3(\text{BO}_3)_4$ crystal, we obtained the values $T_N = 39.42(16)$ and $\beta = 0.369(16)$ ($n = 3$). This value of T_N is slightly higher than the Neel temperature $T_N = 37(1)$ K, known from calorimetric and magnetic measurements on powder samples $\text{YFe}_3(\text{BO}_3)_4$ [13] and neutron diffraction measurements on $\text{YFe}_3({}^{11}\text{BO}_3)_4$ single crystals [53]. This is characteristic of the results of Mössbauer spectroscopy in compounds with a

complex pattern of exchange interactions [37,57]. The values of the parameters β and n found in $\text{YFe}_3(\text{BO}_3)_4$ are characteristic for the three-dimensional Heisenberg model, whereas in the $\text{GdFe}_3(\text{BO}_3)_4$ ferroborate the values of these parameters indicate different non-Heisenberg nature of the ordering at both sites Fe1 ($\beta = 0.33(1)$, $n = 2$) and Fe2 ($\beta = 0.29(2)$, $n = 1$) [37].

Thus, Mössbauer spectroscopy data indicate that the subsystem of iron ions in the $\text{YFe}_3(\text{BO}_3)_4$ crystal is weakly bound to the main crystal lattice, and in the absence of rare-earth ions, forms a fairly uniform three-dimensional magnetic order, that is in good agreement with the results of neutron experiments [53]. Obviously, the formation of a three-dimensional magnetic ordering occurs in one-dimensional structural element - the helicoidal chains of iron ions - due to the active participation of interchain superexchange interactions of Fe-O-O-Fe [58].

4. Summary

XRD structural measurements of the $\text{YFe}_3(\text{BO}_3)_4$ single crystal revealed a temperature-stretched $P3_{121} \leftrightarrow R32$ structural phase transition (presumably of the second order type) in the range of 360–380 K. The results of low-temperature XRD and Mössbauer measurements revealed an anomalous behavior of the unit cell parameter c in the temperature range 30–180 K. It is shown that in the low-temperature phase of $\text{YFe}_3(\text{BO}_3)_4$ (sp.gr. $P3_{121}$), the Mössbauer measurements do not allow to separate the contribution from the two structural sites of iron ions Fe1 and Fe2 even in a magnetically ordered state at temperatures below Neel point. This implies nearly identical structural and magnetic states of iron ions in the sites Fe1 and Fe2 when a nonmagnetic Y occupies the rare-earth sites in the crystal structure of the $\text{RFe}_3(\text{BO}_3)_4$ ferroborates. For the iron ions subsystem, the calculated “Mössbauer” Debye temperature is $\Theta_M = 340(2)$ K, which is three times lower of the Debye temperature of the entire crystal lattice $T_D = 1020$ K. The Mössbauer measurements indicate a relatively weak connection between the helicoidal chains of iron ions and the rest of the crystal lattice. The temperature of the magnetic phase transition $T_N = 39.42(16)$ K is calculated, below which the iron ions form a three-dimensional magnetic order of the Heisenberg type.

Acknowledgments

We thank Dr. A.P. Dudka for help in the low temperature XRD measurements and Dr. D.Yu. Chernyshov for help in the synchrotron XRD measurements. This study was supported by the Federal Agency of Scientific Organizations (Agreement No 007-Г3/43363/26) in parts of energy-dispersive X-ray microanalysis, high-temperature XRD, and Mossbauer measurements, by the Russian Foundation for Basic Research (project #17-02-00766a) in parts of low-temperature XRD and Mossbauer measurements, Russian Ministry of Education and Science and performed using the equipment of the Shared Research Center of the Shubnikov Institute of Crystallography of FSRC “Crystallography and Photonics” RAS.

References

- [1] G.A. Smolenskii, I.E. Chupis, Ferroelectromagnets, Sov. Phys. Usp. 25 (1982) 475–493.
- [2] H. Schmid, Multi-ferroic magnetoelectrics, Ferroelectrics 162 (1994) 317–337.
- [3] D.I. Khomskii, Multiferroics: different ways to combine magnetism and ferroelectrics, J. Magn. Magn. Mater. 306 (2006) 1–8.
- [4] D. Khomskii, Classifying multiferroics: mechanisms and effects, Physics 2 (2009) 20.
- [5] A.P. Pyatakov, A.K. Zvezdin, Magnetoelectric and multiferroic media, Phys. Usp. 55 (2012) 557–581.
- [6] Z. Zhou, Q. Yang, M. Liu, Z. Zhang, X. Zhang, D. Sun, T. Nan, N. Sun, X. Chen,

- Antiferroelectric Materials, Applications and recent progress on multiferroic heterostructures, SPIN 5 (2015) 1530001.**
- [7] H. Palneedi, V. Annappureddy, S. Priya, J. Ryu, Status and perspectives of multiferroic magnetoelectric composite materials and applications, *Actuators* 5 (2016) 9.
- [8] C.-Y. Kuo, Z. Hu, J.C. Yang, S.-C. Liao, Y.L. Huang, R.K. Vasudevan, M.B. Okatan, S. Jesse, S.V. Kalinin, L. Li, H.J. Liu, C.-H. Lai, T.W. Pi, S. Agrestini, K. Chen, P. Ohresser, A. Tanaka, L.H. Tjeng, Y.H. Chu, Single-domain multiferroic BiFeO_3 films, *Nat. Commun.* 7 (2016) 12712.
- [9] V.A. Khomchenko, D.V. Karpinsky, J.A. Paixão, Magnetostructural correlations in BiFeO_3 -based multiferroics, *J. Mater. Chem. C* 5 (2017) 3623–3629.
- [10] M.A. Basith, A. Billah, M.A. Jalil, N. Yesmin, M. Alam Sakib, E.K. Ashik, S.M.E.H. Youssf, S.S. Chowdhury, Md.S. Hossain, S.H. Firoz, B. Ahmad, The 10% Gd and Ti co-doped BiFeO_3 : a promising multiferroic material, *J. Alloys Compd* 694 (2017) 792–799.
- [11] S. Jangra, S. Sanghi, A. Agarwal, M. Rangi, K. Kaswan, S. Khasa, Improved structural, dielectric and magnetic properties of Ca^{2+} and Nb^{5+} co-substituted BiFeO_3 multiferroics, *J. Alloys Compd* 722 (2017) 606–616.
- [12] K. Ramam, B.S. Diwakar, K. Varaprasad, V. Swaminadham, V. Reddy, Magnetic properties of nano-multiferroic materials, *J. Magn. Magn. Mater.* 442 (2017) 453–459.
- [13] M. Balli, B. Roberge, P. Fournier, S. Jandl, Review of the magnetocaloric effect in RMnO_3 and RMn_2O_5 multiferroic crystals, *Crystals* 7 (2017) 44–67.
- [14] H. Sim, J. Oh, J. Jeong, M.D. Le, Je-Geun Park, Hexagonal RMnO_3 : a model system for two-dimensional triangular lattice antiferromagnets, *Acta Cryst. B* 72 (2016) 3–19.
- [15] G. Gamzatov, A.M. Aliev, A.R. Kaul, Magnetocaloric effect in $\text{La}_{1-x}\text{K}_x\text{MnO}_3$ ($x = 0.11, 0.13, 0.15$) composite structures in magnetic fields up to 80 kOe, *J. Alloys Compd* 710 (2017) 292–296.
- [16] H.F. Mohamed, Phase diagram, ac susceptibility and thermoelectric power properties of the $\text{La}_{0.90}\text{Li}_{0.10-x}\text{Na}_x\text{MnO}_3$ manganites, *J. Alloys Compd* 712 (2017) 863–869.
- [17] S.A. Pikin, I.S. Lyubutin, Phenomenological model of multiferroic properties in langasite-type crystals with a triangular magnetic lattice, *Phys. Rev. B* 86 (2012) 064414.
- [18] J.F. Scott, Room-temperature multiferroic magnetoelectrics, *NPG Asia Mater.* 5 (2013) e72.
- [19] Y. Tokura, S. Seki, N. Nagaosa, Multiferroics of spin origin, *Rep. Prog. Phys.* 77 (2014) 076501.
- [20] S. Dong, J.M. Liu, S.W. Cheong, Z. Rend, Multiferroic materials and magnetoelectric physics: symmetry, entanglement, excitation, and topology, *Adv. Phys.* 64 (2015) 519–626.
- [21] M. Fiebig, T. Lottermoser, D. Meier, M. Trassin, The evolution of multiferroics, *Nat. Rev. Mater.* 1 (2016) 16046.
- [22] Shijun Luo, Kefeng Wang, Multiferroicity in cycloidal spiral spin magnet $\beta\text{-CrPO}_4$, *J. Alloys Compd* 726 (2017) 833–836.
- [23] A. Scaramucci, H. Shinaoka, M.V. Mostovoy, M. Müller, C. Mudry, M. Troyer, N.A. Spaldin, Multiferroic magnetic spirals induced by random magnetic exchanges, *Phys. Rev. X* 8 (2018) 011005.
- [24] A.M. Kadomtseva, Yu.F. Popov, G.P. Vorob'ev, A.P. Pyatakov, S.S. Krotov, K.I. Kamilov, V.Yu. Ivanov, A.A. Mukhin, A.K. Zvezdin, A.M. Kuz'menko, L.N. Bezmaternykh, I.A. Gudim, V.L. Temerov, Magnetoelectric and magnetoelastic properties of rare-earth ferroborates, *Low Temp. Phys.* 36 (2010) 511–521.
- [25] S. Hayashida, M. Soda, S. Itoh, T. Yokoo, K. Ohgushi, D. Kawana, H.M. Rønnow, T. Masuda, Magnetic model in multiferroic $\text{NdFe}_3(\text{BO}_3)_4$ investigated by inelastic neutron scattering, *Phys. Rev. B* 92 (2015) 054402.
- [26] T.N. Gaydamak, I.A. Gudim, G.A. Zvyagina, I.V. Bilych, N.G. Burma, K.R. Zhekov, V.D. Fil, Magnetopiezoelectric effect and magnetocapacitance in $\text{SmFe}_3(\text{BO}_3)_4$, *Phys. Rev. B* 92 (2015) 214428.
- [27] A.A. Mukhin, A.M. Kuzmenko, V.Yu. Ivanov, A.G. Pimenov, A.M. Shubaev, V.E. Dziom, Dynamic magnetoelectric phenomena with electromagnons in rare-earth borate multiferroics, *Phys.-Usp* 58 (2015) 993.
- [28] H. Nakajima, T. Usui, Y. Joly, M. Suzuki, Y. Wakabayashi, T. Kimura, Y. Tanaka, Quadrupole moments in chiral material $\text{DyFe}_3(\text{BO}_3)_4$ observed by resonant x-ray diffraction, *Phys. Rev. B* 93 (2016) 144116.
- [29] A. Krylov, E. Moshkina, S. Sofronova, I. Gudim, V. Temerov, A. Vtyurin, Low-temperature features of Raman spectra below magnetic transitions in multiferroic $\text{Ho}_{1-x}\text{Nd}_x\text{Fe}_3(\text{BO}_3)_4$ and $\text{Sm}_{1-y}\text{La}_y\text{Fe}_3(\text{BO}_3)_4$ single crystals, *Ferroelectrics* 509 (2017) 92–96.
- [30] I.V. Golosovsky, A.K. Ovsyanikov, D.N. Aristov, P.G. Matveeva, A.A. Mukhin, M. Boehm, L.-P. Regnault, L.N. Bezmaternykh, Spin-wave dynamics and exchange interactions in multiferroic $\text{NdFe}_3(\text{BO}_3)_4$ explored by inelastic neutron scattering, *J. Magn. Magn. Mater.* 451 (2018) 443–449.
- [31] A.M. Kuzmenko, D. Szaller, Th. Kain, V. Dziom, L. Weymann, A. Shubaev, Anna Pimenov, A.A. Mukhin, V.Yu. Ivanov, I.A. Gudim, L.N. Bezmaternykh, A. Pimenov, Switching of magnons by electric and magnetic fields in multiferroic borates, *Phys. Rev. Lett.* 120 (2018) 027203.
- [32] Y. Hinatsu, Y. Doi, K. Ito, M. Wakeshima, A. Alemi, Magnetic and calorimetric studies on rare-earth iron borates $\text{LnFe}_3(\text{BO}_3)_4$ ($\text{Ln} = \text{Y}, \text{La} - \text{Nd}, \text{Sm} - \text{Ho}$), *J. Solid State Chem.* 172 (2003) 438–445.
- [33] D. Fausti, A.A. Nugroho, P.H.M. van Loosdrecht, S.A. Klimin, M.N. Popova, L.N. Bezmaternykh, Raman scattering from phonons and magnons in $\text{RFe}_3(\text{BO}_3)_4$, *Phys. Rev. B* 74 (2006) 024403.
- [34] V.M. Denisov, L.T. Denisova, I.A. Gudim, V.L. Temerov, N.V. Volkov, G.S. Patrin, L.G. Chumilina, High-temperature heat capacity of $\text{YFe}_3(\text{BO}_3)_4$, *Phys. Solid State* 56 (2014) 276–278.
- [35] I.A. Gudim, E.V. Eremin, V.L. Temerov, Flux growth and spin reorientation in trigonal $\text{Nd}_{1-x}\text{Dy}_x\text{Fe}_3(\text{BO}_3)_4$ single crystals, *J. Cryst. Growth* 312 (2010) 2427–2430.
- [36] I.A. Gudim, E.V. Eremin, M.S. Molokeev, V.L. Temerov, N.V. Volkov, Magnetoelectric polarization of paramagnetic $\text{HoAl}_{3-x}\text{Ga}_x(\text{BO}_3)_4$ single crystals, *Sol. St. Phen.* 215 (2014) 364–367.
- [37] K.V. Frolov, I.S. Lyubutin, E.S. Smirnova, O.A. Alekseeva, I.A. Verin, V.V. Artemov, S.A. Kharlamova, L.N. Bezmaternykh, I.A. Gudim, Low-temperature structural and magnetic phase transitions in multiferroic $\text{GdFe}_3(\text{BO}_3)_4$, *J. Alloys Compd* 671 (2016) 545–551.
- [38] A.P. Dudka, A.M. Antipin, I.A. Verin, New hardware and software platform for experiments on a HUBER-5042 X-ray diffractometer with a DISPLEX DE-202 helium cryostat in the temperature range of 20–300 K, *Crystallogr. Rep.* 62 (2017) 797–801.
- [39] V. Dyadkin, P. Pattison, V. Dmitriev, D. Chernyshov, A new multipurpose diffractometer PILATUS@SNBL, *J. Synchrotron Radiat.* 23 (2016) 825–829.
- [40] P.G. Naumov, I.S. Lyubutin, K.V. Frolov, E.I. Demikhov, A closed-cycle cryostat for optical and Mössbauer spectroscopy in the temperature range 4.2–300 K, *Instrum. Exp. Tech.* 53 (2010) 770–776.
- [41] M.E. Matsnev, V.S. Rusakov, SpectrRelax: an application for Mössbauer spectra modeling and fitting, *AIP Conf. Proc.* 1489 (2012) 178–185.
- [42] N.I. Leonuyk, L.I. Leonuyk, Growth and characterization of $\text{RM}_3(\text{BO}_3)_4$ crystals, *Progr. Cryst. Growth Ch* 31 (1995) 179–278.
- [43] J.A. Campá, C. Cascales, E. Gutiérrez-Puebla, M.A. Monge, I. Rasines, C. Ruiz-Valero, Crystal structure, magnetic order, and vibrational behavior in iron rare-earth borates, *Chem. Mater.* 9 (1997) 237–240.
- [44] M.N. Popova, Spectroscopy of compounds from the family of rare-earth orthoborates, *J. Rare Earth* 27 (2009) 607–611.
- [45] S.A. Klimin, D. Fausti, A. Meetsma, L.N. Bezmaternykh, P.H.M. van Loosdrecht, T.T.M. Palstra, Evidence for differentiation in the iron-helicoidal chain in $\text{GdFe}_3(\text{BO}_3)_4$, *Acta Cryst. B* 61 (2005) 481–485.
- [46] E.S. Smirnova, O.A. Alekseeva, A.P. Dudka, I.A. Verin, V.V. Artemov, L.N. Bezmaternykh, I.A. Gudim, K.V. Frolov, I.S. Lyubutin, Structure of $\text{Gd}_{0.95}\text{Bi}_{0.05}\text{Fe}_3(\text{BO}_3)_4$ single crystals at 293 and 90 K, *Crystallogr. Rep.* 61 (2016) 558–565.
- [47] D.V. Volkov, A.A. Demidov, N.P. Kolmakova, L.V. Takunov, Crystal field effects in rare-earth ferroborates $\text{RFe}_3(\text{BO}_3)_4$ with $\text{R} = \text{Nd}, \text{Tb}, \text{Dy}$, or Er , *Phys. Solid State* 50 (2008) 1677–1680.
- [48] T. Ericsson, R. Wapping, Texture effects in 3/2-1/2 Mössbauer spectra, *J. Phys. Colloques* 37 (C6) (1976) 719–723.
- [49] L. Rebboh, R.D. Desautels, C. Ritter, J.M. Cadogan, V. Temerov, A. Pankrats, J. van Lierop, Short-range correlations and their thermal hysteresis in the paramagnetic phase of $\text{YFe}_3(\text{BO}_3)_4$, *Phys. Rev. B* 83 (2011) 140406(R).
- [50] P. Gülich, E. Bill, A.X. Trautwein (Eds.), *Mössbauer Spectroscopy and Transition Metal Chemistry: Fundamentals and Applications*, Springer, Berlin, Heidelberg, 2011, pp. 81–83.
- [51] R.H. Herber, Structure, Bonding, and the Mossbauer Lattice Temperature, in: R.H. Herber (Ed.), *Chemical Mossbauer Spectroscopy*, Plenum, New York, 1984, pp. 199–205.
- [52] M.A. Chuev, An efficient method of analysis of the hyperfine structure of gamma-resonance spectra using the Voigt profile, *Dokl. Phys.* 438 (2011) 318–322.
- [53] C. Ritter, A. Vorotynov, A. Pankrats, G. Petrakovskii, V. Temerov, I. Gudim, R. Szyszczak, Magnetic structure in iron borates $\text{RFe}_3(\text{BO}_3)_4$ ($\text{R} = \text{Y}, \text{Ho}$): a neutron diffraction and magnetization study, *J. Phys.-Condens Mat* 20 (2008) 365209.
- [54] H.E. Stanley, *Introduction to Phase Transitions and Critical Phenomena*, Clarendon Press, Oxford, 1971, pp. 42–49.
- [55] J.-P. Renard, Magnetic phase transitions in low-dimensional systems, in: P. Delhaes, M. Drillon (Eds.), *Organic and Inorganic Low-dimensional Crystalline Materials*, Plenum Press, New York, London, 1987, pp. 125–140.
- [56] L.J. de Jongh, Introduction to low-dimensional magnetic systems, in: L.J. de Jongh (Ed.), *Magnetic Properties of Layered Transition Metal Compounds*, Kluwer Academic Publishers, Netherlands, 1990, pp. 1–51.
- [57] H. Keller, I.M. Savic, Mössbauer studies of the static and dynamic critical behavior of the layered antiferromagnets RbFe_4 and KFe_4 , *Phys. Rev. B* 28 (1983) 2638.
- [58] C. Ritter, A. Balaev, A. Vorotynov, G. Petrakovskii, D. Velikanov, V. Temerov, I. Gudim, Magnetic structure, magnetic interactions and metamagnetism in terbium iron borate $\text{TbFe}_3(\text{BO}_3)_4$: a neutron diffraction and magnetization study, *J. Phys.-Condens Mat* 19 (2007) 196227.